TLR3 Deficiency in Patients with Herpes Simplex Encephalitis

Shen-Ying Zhang *et al.*

Science **317**, 1522 (2007);
DOI: 10.1126/science.1139522

increase in on-chip parallelism that multicore computing will soon offer. Search-intensive approaches to AI will play an increasingly important role in the evolution of the field.

With checkers finished, the obvious question is whether chess is solvable. Checkers has roughly the square root of the number of positions in chess (somewhere in the 10^{40} to 10^{50} range). Given the effort required to solve checkers, chess will remain unsolved for a long time, barring the invention of new technology. The disk-flipping game of Othello is the next popular game that is likely to be solved, but it will require considerably more resources than were needed to solve checkers (*7*).

References and Notes

1. C. Shannon, *Philos. Mag.* **41**, 256 (1950).
2. "The Duel: Man vs. Machine" (www.rag.de/microsite_chess_com).
3. J. Schaeffer, *One Jump Ahead* (Springer-Verlag, New York, 1997).
4. M. Buro, *IEEE Intell. Syst. J.* **14**, 12 (1999).
5. B. Sheppard, thesis, Universiteit Maastricht, Maastricht, Netherlands (2002).
6. V. Allis, thesis, University of Limburg, Maastricht, Netherlands (1994).
7. J. van den Herik, J. Uiterwijk, J. van Rijswijck, *Artif. Intell.* **134**, 277 (2002).
8. J. Romein, H. Bal, *IEEE Computer* **36**, 26 (2003).
9. K. Appel, W. Haken, *Sci. Am.* **237**, 108 (1977).
10. Chinook Web site, with proof (www.cs.ualberta.ca/~chinook).
11. John's Connect Four Playground (http://homepages.cwi.nl/~tromp/c4/c4.html).
12. R. Gasser, thesis, ETH Zürich, Switzerland (1995).
13. J. Schaeffer *et al.*, "Solving Checkers" (www.ijcai.org/papers/0515.pdf).
14. R. Fortman, *Basic Checkers* (http://home.clara.net/davey/basicche.html).
15. "Longest 10PC MTC" (http://pages.prodigy.net/eyg/Checkers/longest-10pc-mtc.htm).
16. J. Schaeffer *et al.*, in *Advances in Computer Games*, J. van den Herik, H. Iida, E. Heinz, Eds. (Kluwer, Dordrecht, Netherlands, 2003), pp. 193–210.
17. D. Knuth, R. Moore, *Artif. Intell.* **6**, 293 (1975).
18. A. Nagai, thesis, University of Tokyo, Japan (2002).
19. A. Kishimoto, M. Müller, in *Proceedings of the Nineteenth National Conference on Artificial Intelligence* (AAAI Press, Menlo Park, CA, 2004) pp. 644–649.
20. D. Beal, thesis, Universiteit Maastricht, Maastricht, Netherlands (1999).

21. The support of Canada's Natural Sciences and Engineering Research Council (NSERC), Alberta's Informatics Circle of Research Excellence (iCORE), and the Canada Foundation for Innovation is greatly appreciated. Numerous people contributed to this work, including M. Bryant, J. Culberson, B. Gorda, B. Knight, D. Szafron, K. Thompson, and N. Treloar.

Supporting Online Material

www.sciencemag.org/cgi/content/full/1144079/DC1
Materials and Methods
Figs. S1 to S4
References

20 April 2007; accepted 6 July 2007
Published online 19 July 2007;
10.1126/science.1144079
Include this information when citing this paper.

TLR3 Deficiency in Patients with Herpes Simplex Encephalitis

Shen-Ying Zhang,[1,2,3] Emmanuelle Jouanguy,[1,2,3] Sophie Ugolini,[4] Asma Smahi,[5] Gaëlle Elain,[6] Pedro Romero,[7] David Segal,[8] Vanessa Sancho-Shimizu,[1,2] Lazaro Lorenzo,[1,2] Anne Puel,[1,2] Capucine Picard,[1,2,9] Ariane Chapgier,[1,2] Sabine Plancoulaine,[1,2] Matthias Titeux,[10] Céline Cognet,[4] Horst von Bernuth,[1,2] Cheng-Lung Ku,[1,2] Armanda Casrouge,[1,2] Xin-Xin Zhang,[3] Luis Barreiro,[11] Joshua Leonard,[8] Claire Hamilton,[1,2] Pierre Lebon,[12] Bénédicte Héron,[13] Louis Vallée,[14] Lluis Quintana-Murci,[11] Alain Hovnanian,[10] Flore Rozenberg,[12] Eric Vivier,[4] Frédéric Geissmann,[6] Marc Tardieu,[15] Laurent Abel,[1,2] Jean-Laurent Casanova[1,2,3,16]*

Some Toll and Toll-like receptors (TLRs) provide immunity to experimental infections in animal models, but their contribution to host defense in natural ecosystems is unknown. We report a dominant-negative *TLR3* allele in otherwise healthy children with herpes simplex virus 1 (HSV-1) encephalitis. TLR3 is expressed in the central nervous system (CNS), where it is required to control HSV-1, which spreads from the epithelium to the CNS via cranial nerves. TLR3 is also expressed in epithelial and dendritic cells, which apparently use TLR3-independent pathways to prevent further dissemination of HSV-1 and to provide resistance to other pathogens in TLR3-deficient patients. Human TLR3 appears to be redundant in host defense to most microbes but is vital for natural immunity to HSV-1 in the CNS, which suggests that neurotropic viruses have contributed to the evolutionary maintenance of TLR3.

The contribution of Toll and Toll-like receptors to immunity has been studied extensively in the past decade. Toll-deficient *Drosophila* were shown to be susceptible to experimental infections with certain fungi in 1996 (*1*), and a Toll-like receptor 4 (TLR4) null mutation in mice resistant to lipopolysaccharide (LPS) but susceptible to certain Gram-negative bacteria was identified in 1998 (*2*). Mice deficient for individual TLRs have since been generated and shown to have diverse infectious phenotypes, from susceptibility to resistance, depending on the TLR-pathogen combination (*3*). However, it remains unclear whether TLRs play nonredundant roles—beneficial or detrimental—in natural, as opposed to experimental, infections. This biological question is important, because natural selection acts on a given species in the setting of natural (rather than experimental) ecosystems. The human model is particularly suitable for analyses of the relevance of genes such as those of TLRs to host defense in natural ecosystems (*4*). Nevertheless, although many studies have suggested that TLR genes are involved in human infectious diseases, this has not been unambiguously demonstrated (*5*). In particular, no primary immunodeficiency involving TLRs has been identified.

The discovery of inherited interleukin 1 receptor-associated kinase-4 (IRAK-4) deficiency in children with bacterial diseases implicated human TLRs, interleukin-1 receptors (IL-1Rs), or both in host defense (*6*, *7*). However, the narrow range of infections documented in such patients indicates that IRAK-4–dependent, TLR-mediated immunity is redundant for protective immunity to most microbes. In particular, IRAK-4–deficient patients are not susceptible to herpes simplex virus 1 (HSV-1) encephalitis (HSE). In HSE, HSV-1 infects epithelial cells in the oral and nasal mucosa and progresses to the central nervous system (CNS) via the trigeminal or olfactory nerves (*8*). A genetic etiology of HSE was found in two children who lacked functional UNC-93B (*9*), an endoplasmic reticulum protein required for TLR3, TLR7, TLR8, and TLR9 signaling (*10*). Both UNC-93B– and IRAK-4–deficient patients fail to signal through TLR7, TLR8, and TLR9, but unlike IRAK-4–deficient patients (*7*), UNC-93B–deficient patients display impaired TLR3-dependent interferon-α (IFN-α) -β, and -λ production (*9*). Moreover, HSV-1 is a double-stranded DNA virus with double-stranded RNA (dsRNA) intermediates (*11*), and TLR3 recog-

[1]Human Genetics of Infectious Diseases, Institut National de la Santé et de la Recherche Médicale (INSERM), U550, Faculty Necker, Paris 75015, France. [2]University Paris René Descartes, Paris 75015, France. [3]French-Chinese Laboratory of Genetics and Life Sciences, Rui Jin Hospital, Shanghai Jiao Tong University, Shanghai 200025, China. [4]Marseille-Luminy Immunology Institute, Marseille 13288, France. [5]Department of Genetics, INSERM, U781, Necker Hospital, Paris 75015, France. [6]Laboratory of Mononuclear Cell Biology, INSERM, U838, Necker Hospital, Paris 75015, France. [7]Ludwig Institute for Cancer Research, Lausanne Branch, University Hospital, Lausanne 1005, Switzerland. [8]Experimental Immunology Branch, National Cancer Institute, National Institutes of Health, Bethesda, MD 20892, USA. [9]Center for the Study of Immunodeficiencies, Necker Hospital, Paris 75015, France. [10]INSERM, U563, University Toulouse Paul Sabatier, Toulouse 31000, France. [11]Centre National de la Recherche Scientifique, URA3012, Pasteur Institute, Paris 75015, France. [12]Virology, Cochin-Saint-Vincent de Paul Hospital, University Paris René Descartes, Paris 75014, France. [13]Pediatric Neurology, Trousseau Hospital, Paris 75012, France. [14]Pediatric Neurology, University Hospital, Lille 59037, France. [15]Pediatric Neurology, Bicêtre Hospital, University Paris Sud, Kremlin-Bicêtre 94270, France. [16]Pediatric Hematology-Immunology, Necker Hospital, Paris 75015, France.

*To whom correspondence should be addressed. E-mail: casanova@necker.fr

nizes dsRNA (*12*). Finally, TLR3 is expressed in CNS-resident cells (*13*–*15*) and peripheral nerves (*16*). Collectively, these observations suggest that impaired TLR3-dependent induction of IFN-α, -β and -λ might be involved in HSE.

A heterozygous TLR3 mutation in two children with HSE. We investigated two unrelated French children (P1 and P2) with HSE (SOM Text, note 2). UNC-93B deficiency was excluded on genetic and immunological grounds (fig. S1, A to D). Leukocytes and fibroblasts from P1 and P2 harbored the same heterozygous substitution (C→T) in *TLR3* at nucleotide position 1660 (c.1660C>T) (Fig. 1, A and B). The two kindreds represent independent mutational events because the two P554S mutations were in different *TLR3* haplotypes. The mutation leads to the replacement of a proline (P) by a serine (S) at residue 554 (P554S) (Fig. 1C). P554S has not previously been described (*17*, *18*) and was not found in any of the 1581 unrelated healthy individuals examined (3162 chromosomes), including 241 Europeans. Residue P554 of TLR3 is conserved in the 18 animal species studied (Fig. 1D). The extracellular, ligand-binding domain of TLR3 contains 23 contiguous leucine-rich repeats (LRRs) forming a large, horseshoe-shaped solenoid (Fig. 1E) (*19*). P554 anchors the TLR3-specific insertion of residues 544 to 554 in LRR20 (Fig. 1E) (*19*, *20*). This region is thought to be critical for dsRNA binding to TLR3 (*20*) and TLR3 multimerization (*19*). Three relatives of P1 and two of P2 were also heterozygous for the mutation (Fig. 1A). They were HSV-1 seropositive but had not suffered from HSE, which suggests that the P554S TLR3 mutation conferred an autosomal dominant predisposition to HSE with incomplete clinical penetrance.

Impaired responsiveness of fibroblasts to poly(I:C) stimulation. We derived dermal fibroblastic cell lines, which selectively express TLR3 (*9*), from patients and controls. The TLR3 agonist polyinosine-polycytidylic acid [poly(I:C)], which mimics dsRNA (*12*), induced IFN-β, -λ, and IL-6 in a dose- and time-dependent manner in all control fibroblasts but not in the TLR3-deficient fibrosarcoma P2.1 cell line (SOM Text, note 1) (Fig. 2A and fig. S2A). Primary and simian virus 40 (SV40)–transformed fibroblasts from P1 and P2 displayed only a residual response at high concentrations of poly(I:C) and late time points (Fig. 2A). IL-6 induction was less impaired. The induction of IFN-β and -λ mRNA production by poly(I:C) was markedly weaker in P1 fibroblasts (fig. S2B). Both nuclear factor kappa B (NF-κB) (Fig. 2B) and IFN regulatory factor-3 (IRF-3) (Fig. 2C) activation were impaired in response to poly(I:C) in the patients' fibroblasts, which responded normally to tumor necrosis factor–α (TNF-α) and IL-1β (Fig. 2B and fig. S2C). NF-κB essential modulator (NEMO)–deficient fibroblasts (SOM Text, note 1) did not respond to poly(I:C), IL-1β, or TNF-α (Fig. 2B), and UNC-93B–deficient fibroblasts (*9*) did not respond to poly (I:C) (Fig. 2C). Finally, all tested relatives carrying the TLR3 mutation, but none of the relatives without this mutation, displayed impaired responses to poly(I:C) (fig. S2D). The cosegregation of genotype and fibroblastic phenotype suggests that heterozygosity for the P554S *TLR3* allele confers autosomal dominant hyporesponsiveness to poly(I:C) in fibroblasts.

Dominant-negative effect of the P554S *TLR3* allele in fibroblasts. TLR3 multimerizes upon binding dsRNA, and several TLR3 mutants are dominant negative (*20*–*22*), which suggests that the P554S mutation may be dominant negative. *TLR3* mRNA is produced in normal quantities (Fig. 2D) in the patients' fibroblasts (fig. S2E), and the wild-type (WT) and P554S *TLR3* mRNAs were equally abundant (fig. S2F). Stable transfection of P2.1 cells with C-terminal

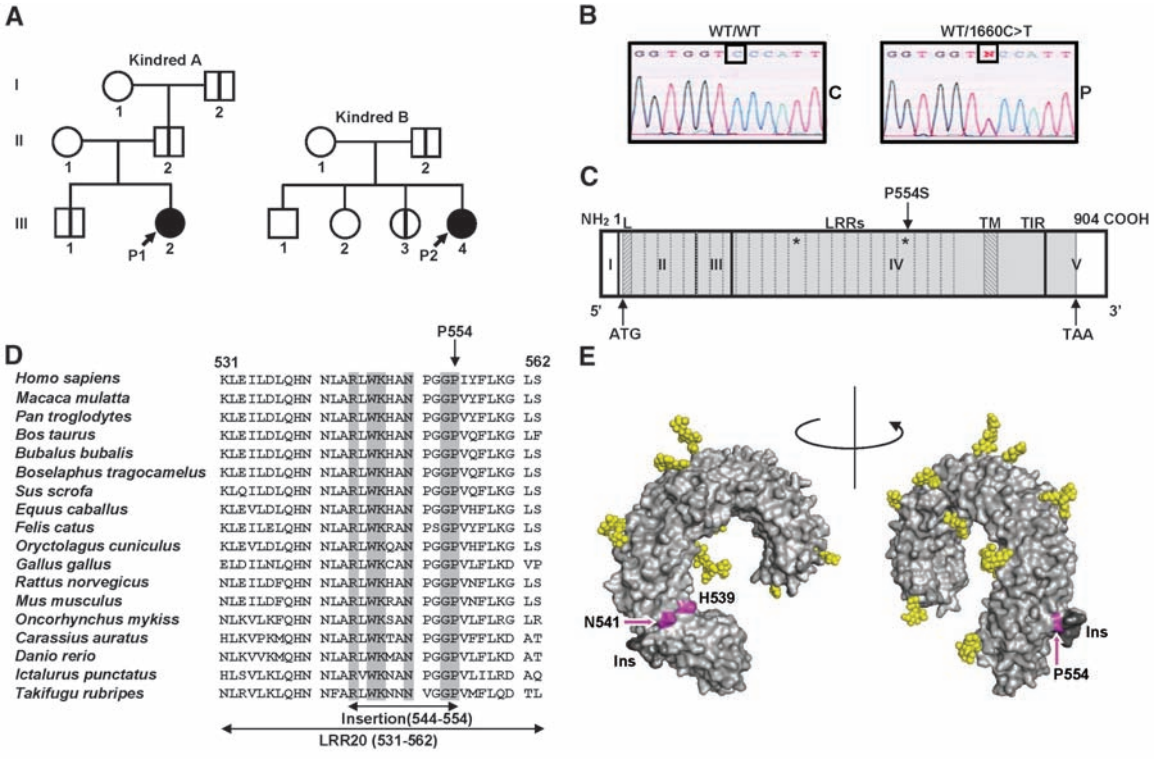

Fig. 1. Heterozygous TLR3 P554S mutation in two unrelated children with HSE. (**A**) Family pedigrees, with allele segregation in the two families. The patients, in black, are heterozygous for the mutation. The other family members heterozygous for the mutation are indicated by bold vertical lines. (**B**) Heterozygous c.1660C>T mutation in the patients. The sequence of the polymerase chain reaction products of genomic DNA from leukocytes of a control (C) and P1 (P) is shown. The mutation was confirmed in genomic DNA and cDNA from leukocytes and fibroblasts. (**C**) Schematic representation of *TLR3* gene structure. Human *TLR3* has five exons (Roman numerals) encoding a protein (shown in gray) composed of a leader sequence (L), an LRR domain, a transmembrane (TM) domain, and a Toll/interleukin-1 receptor (TIR) domain. The various LRR motifs, the N-terminal cap, and the C-terminal cap of the LRR domain are separated by dotted vertical lines, and the two LRRs with an insertion are indicated by asterisks. The c.1660C>T mutation results in a proline (P) to serine (S) substitution at amino acid position 554 (P554S) in LRR20. (**D**) LRR20 of TLR3 in humans and the corresponding region in the other 17 species studied, with the insertion indicated. The amino acids conserved in the insertion in all these species are shaded in gray. (**E**) Two views of the human TLR3 ectodomain (ECD) surface. H539 and N541 (left), implicated in ligand binding, and P554 (right) are shown in magenta. "Ins" refers to the eight residues from W546 to G553 in the TLR3-specific insertion 544 to 554 of the LRR20, and is shown in dark gray. Glycan is shown in yellow, and the C terminus of the TLR3 ECD is at the bottom.

hemagglutinin (HA)–tagged WT *TLR3*, but not with P554S *TLR3*, restored the cell response to poly(I:C), as measured by IFN-β (fig. S2G) and IFN-λ production (Fig. 2E). Both WT and P554S *TLR3* mRNAs were detected (Fig. 2F). The P554S TLR3 protein had a lower molecular weight than the WT, as shown by Western blotting with two antibodies that specifically recognize the TLR3 N-terminal ectodomain, but not with an antibody to C-terminal–tagged HA (Fig. 2G). Upon transient transfection of control fibroblasts with various ratios of mock vector and P554S *TLR3* allele, the response to poly(I:C) decreased as the proportion of P554S *TLR3* allele increased (fig. S2H). Moreover, control fibroblasts stably transfected with the P554S *TLR3* allele lost their ability to respond to poly(I:C) (Fig. 2H). These observations were extended to P2.1 recipient cells (SOM Text, note 3). The P554S TLR3 protein is thus C-terminally truncated, loss-of-function for poly(I:C) responsiveness, and dominant negative in dermal fibroblasts and the fibrosarcoma P2.1 cell line, at least for IFN induction.

Impaired IFN-dependent control of viruses in TLR3-deficient fibroblasts. UNC-93B–deficient fibroblasts produce little IFN-β and -λ upon viral stimulation, resulting in high levels of viral replication and cell death (*9*). We therefore infected TLR3-heterozygous fibroblasts with HSV-1 and another neurotropic virus, vesicular stomatitis virus (VSV)—a highly cytopathic virus and potent IFN inducer in human fibroblasts. IFN-β and -λ production after infection with VSV and HSV-1 was markedly weaker in fibroblasts from the patients than in those from controls (Fig. 3, A and B). Six hours after VSV infection, viral replication rates were higher in P1 cells—as in Stat-1–deficient (*23*) and UNC-93B–deficient (*9*) cells—than in controls (Fig. 3C). Cell survival was also markedly lower for the patients than the controls and was similar to that for UNC-93B– and Stat-1–deficient cells after 24 hours of VSV and 96 hours of HSV-1 infection (Fig. 3D). Treatment with IFN-α or IFN-β complemented the phenotype of TLR3- and UNC-93B–deficient, but not Stat-1–deficient, cells (Fig. 3, C and E) in a dose-dependent manner (fig. S3). IFN-λ also partially complemented the phenotype, albeit less effectively than IFN-α or IFN-β (Fig. 3E). Our results thus demonstrate a causal relationship between heterozygosity for the P544S TLR3 mutation, impaired TLR3 signaling, abnormally weak IFN-α/β and -λ production, enhanced viral replication, and higher levels of fibroblast cell death upon viral infection.

Impaired response to poly(I:C) stimulation in MDDCs, NK, and CD8 T cells. Monocyte-derived dendritic cells (MDDCs) (*24*) from P1 and the third sibling of P2 (S3-P2), both heterozygous for the TLR3 mutation, responded more weakly than

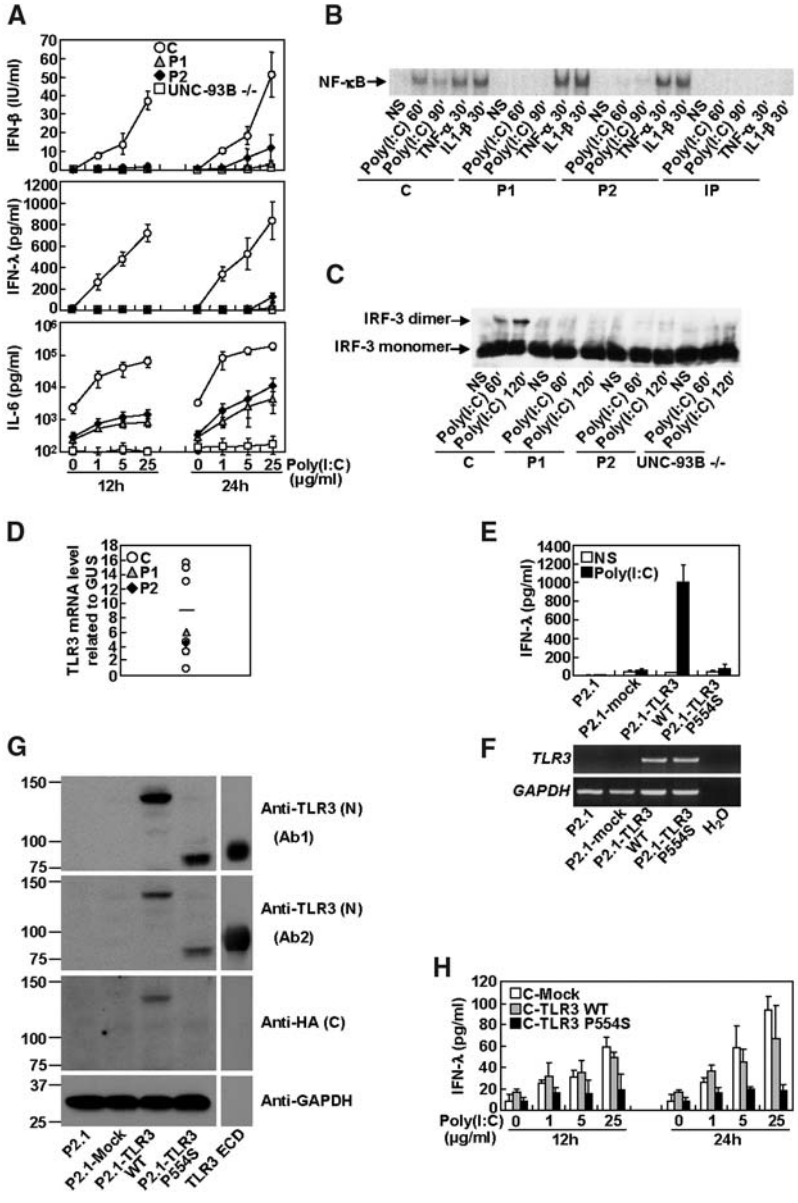

Fig. 2. Impaired response to poly(I:C) of fibroblasts and dominant-negative effect of the *TLR3* P554S allele in fibroblasts (**A**) IFN-β, -λ, and IL-6 production in SV40-transformed fibroblasts (SV40 fibroblasts) from a control (C), P1, P2, and a UNC-93B–deficient (UNC-93B$^{-/-}$) patient upon stimulation with various doses of poly(I:C) for 12 or 24 hours. (**B**) NF-κB-DNA–binding activity of nuclear extracts from the SV40 fibroblasts of a control (C), P1, P2, and a NEMO-deficient (IP) patient upon TNF-α and IL-1β stimulation for 30 min, or poly(I:C) stimulation for 60 min or 90 min, as assessed by electrophoretic mobility shift assay. The experiment is representative of two. (**C**) IRF-3 monomers and dimers in total cell extracts from SV40 fibroblasts of a control (C), P1, P2, and a UNC-93B$^{-/-}$ patient, upon poly(I:C) stimulation for 1 or 2 hours, as assessed by Western blotting. (**D**) *TLR3* mRNA levels in SV40 fibroblasts from six controls (C) [mean value indicated by (—)], P1, and P2; β-glucuronidase (GUS) was used for normalization. The experiment shown is representative of two. (**E** to **G**) In P2.1 cell lines not transfected (P2.1) or stably transfected with pUNO expression vectors carrying no insert (P2.1-mock), or the C-terminal HA-tagged *TLR3* cDNA with the WT sequence (P2.1-TLR3 WT) or with the P554S mutation (P2.1-TLR3 P554S), IFN-λ production (E) was measured after 24 hours stimulation with poly(I:C). The *TLR3* cDNA in these cells (F) is shown, with the internal amplification control *GAPDH*; the experiment shown is representative of three. TLR3 expression in these cells (G) was assessed by Western blotting, using two antibodies to N-terminal TLR3 [anti-TLR3 (N) Ab1 and anti-TLR3 (N) Ab2] and an antibody to C-terminal–tagged HA. The experiment shown is representative of six. The recombinant TLR3 ECD protein was used as a positive control for the antibody. The internal expression control was glyceraldehyde-phosphate dehydrogenase (GAPDH). (**H**) IFN-λ production, in a control SV40-fibroblast cell line, stably transfected with an empty vector (C-mock), a C-terminal HA-tagged pUNO-TLR3 WT vector (C-TLR3 WT), or an HA-tagged pUNO-TLR3 vector containing the P554S mutation (C-TLR3 P554S) upon stimulation with various doses of poly(I:C) for 12 or 24 hours. In (A), (E) and (H), the production of IFNs and IL-6 was measured by enzyme-linked immunosorbent assay (ELISA). Mean values ±SD were calculated from three independent experiments.

control cells to poly(I:C) but responded normally to LPS and R-848 in terms of IFN-β, IFN-λ, and IL-12p40 production (Fig. 4A) and CD40, CD80, and CD86 up-regulation (fig. S4A). We tested leukocyte subsets ex vivo to gain further insight into HSE pathogenesis. Unlike purified natural killer (NK) cells from controls (*25*), the patients' NK cells barely responded to poly(I:C) (Fig. 4B) but responded normally to K562 (Fig. 4B and SOM Text, note 4). Nevertheless, the known patients with inherited NK deficiency were not prone to HSE (*9*, *26*). We did not test γ/δ T cells, but unlike CD8 α/β T cells (*27*) from controls, cells from P2 and her father, both heterozygous for the P554S mutation, responded weakly to poly(I:C) costimulation (fig. S4C) but normally to costimulation with CD28 (fig. S4C). However, the known CD8- and HLA-I–deficient patients did not present HSE (*28*). Although affected by the TLR3 mutation, the contribution of NK and CD8 T cells to the pathogenesis of HSE in TLR3-heterozygous children is probably modest.

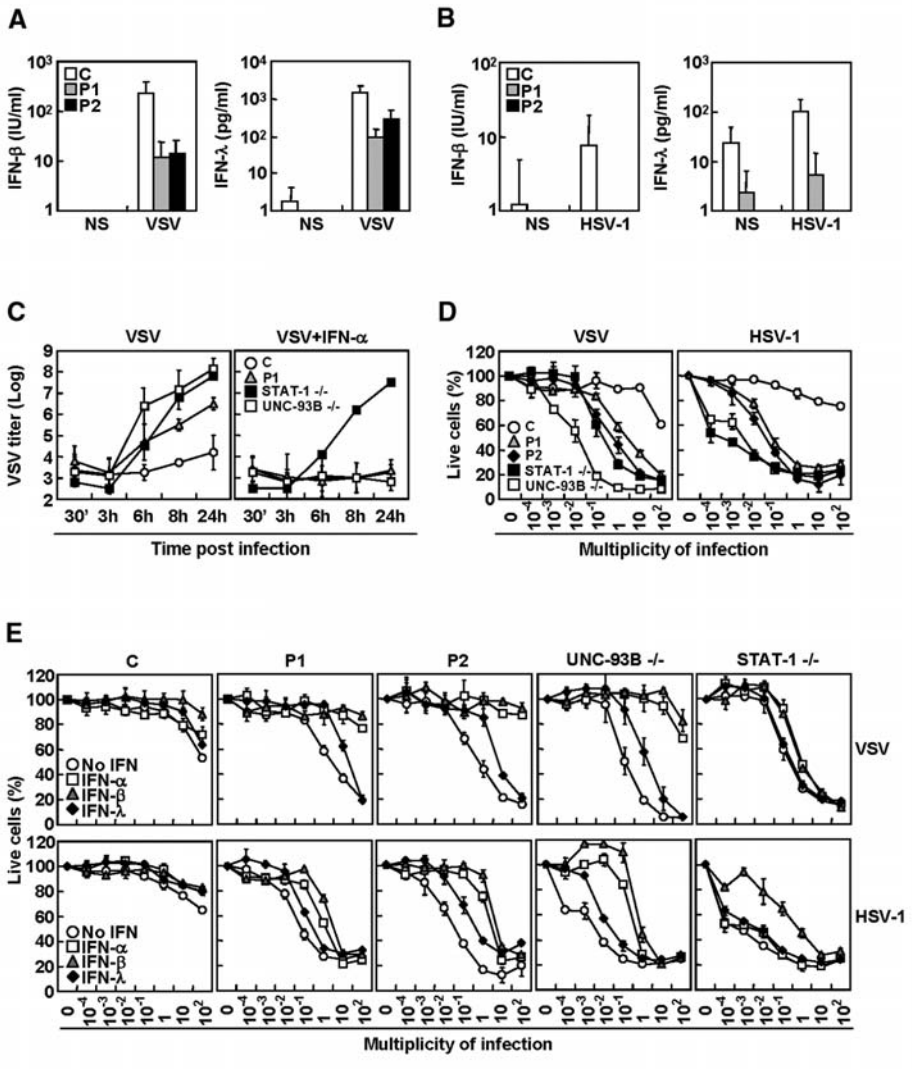

Fig. 3. High levels of viral replication and cell mortality in fibroblasts from the patients and rescue by treatment with IFN-α, -β, -λ. (**A** and **B**) IFN-β and -λ production, measured by ELISA, by SV40 fibroblasts from controls (C), P1, and P2 after 24 hours of VSV (A) or HSV-1 (B) stimulation. Mean values ±SD were calculated from six independent experiments with three different controls. (**C**) VSV titers, estimated on Vero cells, in SV40 fibroblasts from healthy controls (C), P1, a UNC-93B$^{-/-}$ patient, and a Stat1-deficient (Stat1$^{-/-}$) patient, at various times after VSV infection with or without 18 hours of pretreatment with IFN-α. Mean values ±SD of two independent experiments with two different controls are shown. (**D** and **E**) Live cell percentages, estimated by resazurin oxidation/reduction, for SV40 fibroblasts from a healthy control (C), P1, P2, a UNC-93B$^{-/-}$, and a Stat-1$^{-/-}$ patient, 24 and 96 hours after infection with various multiplicities of infection of VSV and HSV-1. The cells either were not treated (D), or were subjected to pretreatment (E) for 18 hours with recombinant IFN-α, -β or -λ and with IFN-α, -β or -λ present during infection. Mean values ±SD were calculated for three replicates in each experiment; one representative of three experiments with two different controls is shown.

Response of blood DCs and keratinocytes to poly(I:C) stimulation. Like IRAK-4– and UNC-93B–deficient peripheral blood mononuclear cells (PBMCs) (*7*, *9*), the patients' cells responded normally to poly(I:C) in terms of IFN-α, -β and -λ production (fig. S1, A to C, and fig. S5A). The patients' purified myeloid DCs (MDCs) (*24*) responded normally to poly(I:C) in terms of IFN-λ production (Fig. 4C). Moreover, IFN-α (Fig. 4D) and -λ (fig. S5B) were produced by poly(I:C)-stimulated purified plasmacytoid DCs (PDCs) from patients and controls, although PDCs are not thought to express TLR3 (*24*). The lack of clinical HSV-1 dissemination, particularly by the blood, in patients with HSE may therefore be due to the induction of IFNs by MDCs and PDCs stimulated with dsRNA or other viral intermediates (*29*). HSV-1 also does not spread to epithelia during or following HSE (*9*). Several epithelial cell types, keratinocytes in particular (*30*), express TLR3 and respond to poly(I:C). TLR3-heterozygous keratinocytes from P2 did not respond to poly(I:C), as shown by measurements of IL-6 secretion (Fig. 4E). However, they responded to poly(I:C), as shown by IFN-λ (Fig. 4E) and IL-8 (fig. S5C) production. The IFN-λ response of the patients' keratinocytes suggested that the sensing of dsRNA and, possibly, other viral intermediates (*29*) in epithelial cells prevented the epithelial dissemination of HSV-1 in TLR3-heterozygous patients with HSE. The poly(I:C) responsiveness of DCs and keratinocytes probably operated through TLR3-independent pathways (*29*), although we cannot exclude the possibility of residual TLR3 signaling or a lack of dominance of the P554S TLR3 mutant in such cells.

Most viruses trigger IFNs in TLR3 heterozygous cells. The lack of other severe viral diseases in TLR3-heterozygous and UNC-93B–deficient patients with HSE is intriguing (*9*, *31*). Our demonstration of poly(I:C) responsiveness in keratinocytes and blood DCs is important because most viruses enter the host via the epithelium, and most forms of human viral encephalitis other than HSE and rabies are blood-borne. We then stimulated the patients' blood cells with 11 viruses (*7*, *9*). TLR3-deficient PBMCs displayed normal production of IFN-α, -β and -λ, and other cytokines in response to the viruses tested (Fig. 4F and fig. S5D). Similarly, cells from IRAK-4–deficient patients showed normal or weak but detectable responses to all viruses (*7*). Cells from UNC-93B–deficient patients showed impaired, but not abolished, responses to several viruses, including HSV-1 (*9*). We then tested the responses of the patients' fibroblasts to the six viruses that stimulated IFN-β and -λ production in control fibroblasts. Like IRAK-4–deficient fibroblasts (*7*), both TLR3-deficient and UNC93-B–deficient fibroblasts responded well to four of the viruses, but unlike the IRAK-4–deficient fibroblasts (*7*), they responded poorly to HSV-1 and VSV (Fig. 4G). The in-

duction of IFN-α, -β, and -λ in blood cells and fibroblasts from TLR3-heterozygous patients, after stimulation with most of the viruses tested, was consistent with the natural resistance of these patients to most viruses other than HSV-1.

Concluding remarks. After autosomal recessive UNC-93B deficiency (*9*), autosomal dominant TLR3 deficiency is the second genetic etiology of isolated HSE to be identified. Because Stat-1–deficient (*32*) patients are also prone to HSE (and other infectious diseases), the molecular pathogenesis of HSE primarily involves impaired TLR3-dependent, IFN-α, -β, and -λ responses. Several lines of evidence also indicate that the pathogenic cellular mechanism underlying HSE in TLR3-heterozygous patients involves an intrinsic defect affecting CNS-resident cells: the neurotropic infection of the CNS by HSV-1, the CNS-restricted clinical course of HSE, the widespread and preferential expression of TLR3 in the CNS, the poly(I:C)–inducible production of antiviral IFNs by blood DCs in TLR3 heterozygotes, and the absence of HSE in patients with conventional primary immunodeficiencies. In addition to revealing the pathogenic mechanism and a basis for both molecular diagnosis and genetic counseling, our findings provide further support for the treatment of HSE patients with IFN-α in addition to acyclovir (*9*). Interestingly, five of the seven TLR3-deficient individuals and one of the three UNC-93B–deficient individuals did not develop HSE after HSV-1 infection. The incomplete clinical penetrance of TLR3 and UNC-93B deficiency is consistent with the typically sporadic, as opposed to familial, occurrence of HSE (*8*, *9*). Multiple factors may affect clinical penetrance, including age at infection with HSV-1, the viral inoculum, and human modifier genes.

The infection of TLR3-deficient mice with HSV-1 has not yet been reported, but mouse TLR3 appears to be largely redundant in antiviral immunity. TLR3-deficient mice are susceptible to encephalomyocarditis virus (EMCV) (*33*) and mouse cytomegalovirus (MCMV) (*34*, *35*), at least in some experimental conditions and, to a lesser extent, to respiratory syncytial virus (RSV) (*36*). However, TLR3-deficient mice have normal resistance to lymphocytic choriomeningitis virus

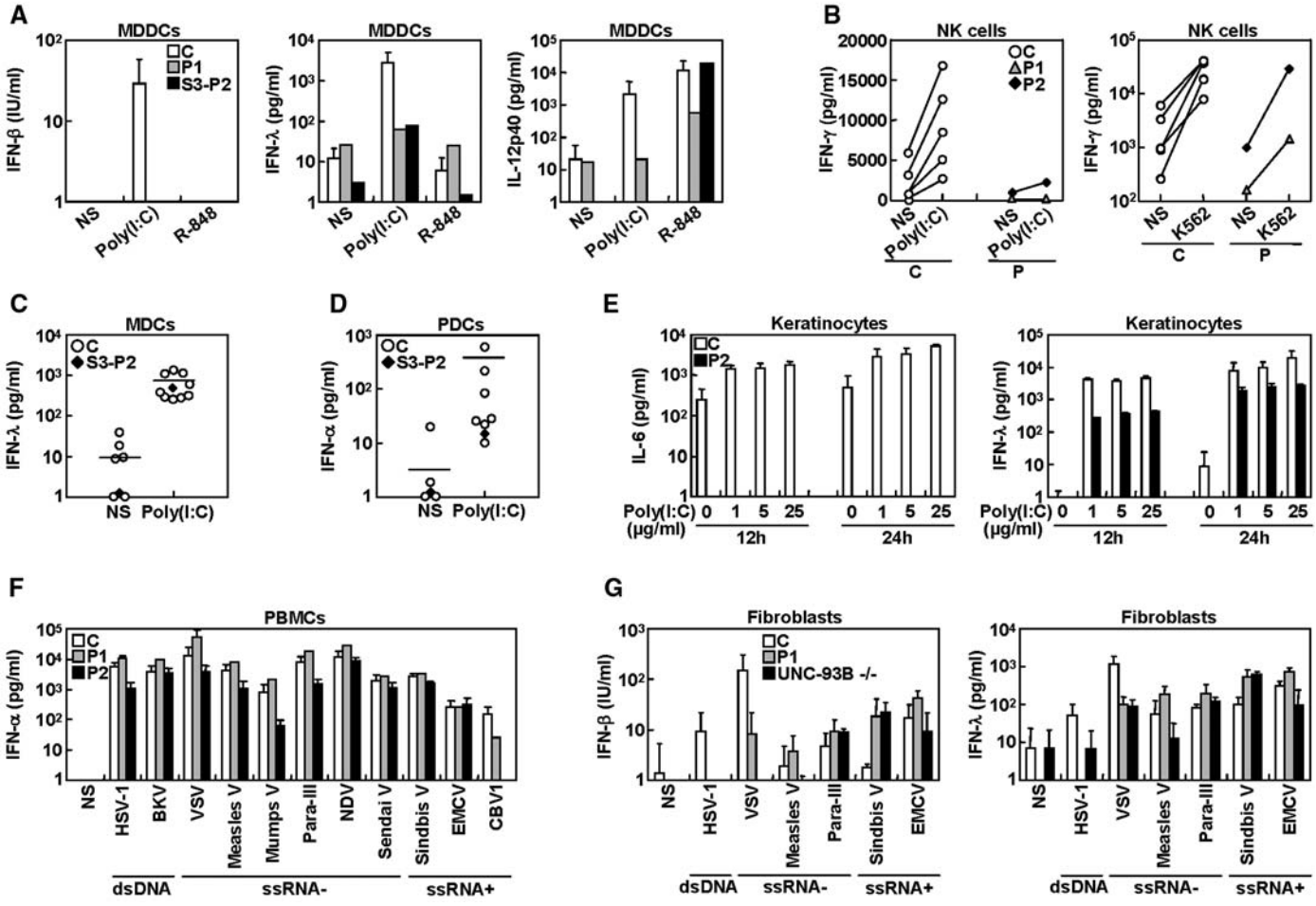

Fig. 4. Impaired response to poly(I:C) in MDDCs and NK cells but not in blood DCs and keratinocytes; most viruses trigger IFNs in TLR3 heterozygous blood and fibroblasts (**A**) IFN-β, -λ, and IL-12p40 production, by MDDCs from controls (C), P1, and a sister of P2 (S3-P2) heterozygous for the P554S mutation. Mean values ±SD were calculated from the data for 12 controls. (**B**) IFN-γ production, in purified NK cells from five controls (C), P1, and P2, upon stimulation with poly(I:C) or K562 for 24 hours in the presence of IL-12. (**C**) IFN-λ production in MDCs from eight controls (C) [mean value indicated by (—)] and a sister of P2 (S3-P2) heterozygous for the P554S mutation. (**D**) IFN-α production, in PDCs from seven controls (C) [mean value indicated by (—)] and S3-P2. (**E**) IL-6 and IFN-λ production by keratinocytes from controls (C) and P2. Mean values ±SD were calculated for two replicates in each experiment, with two different controls. (**F**) IFN-α production by PBMCs 24 hours after stimulation with intact viruses. Means ±SD were calculated for the controls (C) from data for six healthy individuals, each tested once, for P1 (tested four times for HSV-1 and VSV and once for the other viruses), and for P2 (tested twice for all the viruses). (**G**) IFN-β and -λ production, 24 hours after stimulation with intact viruses, in fibroblasts from controls, P1, and a UNC-93B$^{-/-}$ patient. Mean values ±SD were calculated from three independent experiments with two different controls. The production of IFNs and IL-6 was measured by ELISA in (A) to (G).

(LCMV), VSV, and reovirus (*35*). Moreover, TLR3-deficient mice are resistant to influenza A virus (*37*), West Nile virus (*38*), and phlebovirus (*39*). Human TLR3 also appears to be largely redundant for antiviral immunity, as the known TLR3- and UNC-93B–deficient patients have had infections with numerous viruses without developing severe disease (*9*, *31*). Nevertheless, human TLR3 is essential for primary immunity to HSV-1 in the CNS, at least in some circumstances. Our study provides conclusive evidence that an individual TLR can play a nonredundant role in host defense in the setting of a natural ecosystem. Given its ability to recognize dsRNA, human TLR3 may have been of evolutionary importance: Most patients with HSE died until the advent of acyclovir in 1981 (*8*). As naturally occurring mutations in TLR3 may be dominant negative, it is tempting to speculate that HSV-1 and other neurotropic viruses may have exerted direct selective pressure, driving the maintenance of human TLR3.

References and Notes

1. B. Lemaitre, E. Nicolas, L. Michaut, J. M. Reichhart, J. A. Hoffmann, *Cell* **86**, 973 (1996).
2. A. Poltorak *et al.*, *Science* **282**, 2085 (1998).
3. S. Akira, S. Uematsu, O. Takeuchi, *Cell* **124**, 783 (2006).
4. J.-L. Casanova, L. Abel, *Science* **317**, 617 (2007).
5. S. E. Turvey, T. R. Hawn, *Clin. Immunol.* **120**, 1 (2006).
6. C. Picard *et al.*, *Science* **299**, 2076 (2003).
7. K. Yang *et al.*, *Immunity* **23**, 465 (2005).
8. R. J. Whitley, *Antiviral Res.* **71**, 141 (2006).
9. A. Casrouge *et al.*, *Science* **314**, 308 (2006).
10. K. Tabeta *et al.*, *Nat. Immunol.* **7**, 156 (2006).
11. B. Jacquemont, B. Roizman, *J. Virol.* **15**, 707 (1975).
12. L. Alexopoulou, A. C. Holt, R. Medzhitov, R. A. Flavell, *Nature* **413**, 732 (2001).
13. M. Bsibsi, R. Ravid, D. Gveric, J. M. van Noort, *J. Neuropathol. Exp. Neurol.* **61**, 1013 (2002).
14. C. S. Jack *et al.*, *J. Immunol.* **175**, 4320 (2005).
15. C. Prehaud, F. Megret, M. Lafage, M. Lafon, *J. Virol.* **79**, 12893 (2005).
16. H. Lee *et al.*, *Glia* **55**, 712 (2007).
17. F. Hidaka *et al.*, *Clin. Immunol.* **119**, 188 (2006).
18. C. T. Ranjith-Kumar *et al.*, *J. Biol. Chem.* **282**, 17696 (2007).
19. J. Choe, M. S. Kelker, I. A. Wilson, *Science* **309**, 581 (2005).
20. J. K. Bell, J. Askins, P. R. Hall, D. R. Davies, D. M. Segal, *Proc. Natl. Acad. Sci. U.S.A.* **103**, 8792 (2006).
21. C. T. Ranjith-Kumar *et al.*, *J. Biol. Chem.* **282**, 7668 (2007).
22. O. de Bouteiller *et al.*, *J. Biol. Chem.* **280**, 38133 (2005).
23. A. Chapgier *et al.*, *J. Immunol.* **176**, 5078 (2006).
24. A. Iwasaki, R. Medzhitov, *Nat. Immunol.* **5**, 987 (2004).
25. K. N. Schmidt *et al.*, *J. Immunol.* **172**, 138 (2004).
26. C. Eidenschenk *et al.*, *J. Immunol.* **177**, 8835 (2006).
27. J. Tabiasco *et al.*, *J. Immunol.* **177**, 8708 (2006).
28. V. Cerundolo, H. de la Salle, *Semin. Immunol.* **18**, 330 (2006).
29. E. Meylan, J. Tschopp, *Mol. Cell* **22**, 561 (2006).
30. M. C. Lebre *et al.*, *J. Invest. Dermatol.* **127**, 331 (2006).
31. J. L. Casanova, L. Abel, *Nat. Rev. Immunol.* **4**, 55 (2004).
32. S. Dupuis *et al.*, *Nat. Genet.* **33**, 388 (2003).
33. H. S. Hardarson *et al.*, *Am. J. Physiol. Heart Circ. Physiol.* **292**, H251 (2006).
34. K. Tabeta *et al.*, *Proc. Natl. Acad. Sci. U.S.A.* **101**, 3516 (2004).
35. K. H. Edelmann *et al.*, *Virology* **322**, 231 (2004).
36. B. D. Rudd *et al.*, *J. Immunol.* **176**, 1937 (2006).
37. R. Le Goffic *et al.*, *PLoS Pathog.* **2**, e53 (2006).
38. T. Wang *et al.*, *Nat. Med.* **10**, 1366 (2004).
39. B. B. Gowen *et al.*, *J. Immunol.* **177**, 6301 (2006).

40. We thank the members of the Laboratory of Human Genetics of Infectious Diseases, as well as P. Benaroch, S. Amigorena, K. Honda, T. Taniguchi, F. Barrat, R. Miller, L. Zitvogel, S. Matikainen, and D. W. Leaman for helpful discussions or reagents. We thank the children and their families for their participation in this study, which was supported by the Schlumberger Foundation, the BNP-Paribas Foundation, the Groupement d'Intérêt Scientifique Maladies Rares, the Action Concertée Incitative de Microbiologie, The March of Dimes, and the Action Nationale pour la Recherche. P.R. is supported by a European Union FP6 grant. J.-L.C. is an international scholar of the Howard Hughes Medical Institute.

Supporting Online Material

www.sciencemag.org/cgi/content/full/317/5844/1522/DC1
Materials and Methods
SOM Text
Figs. S1 to S5
References

4 January 2007; accepted 2 August 2007
10.1126/science.1139522

Lighting the Universe with Filaments

Liang Gao[1]* and Tom Theuns[1,2]

The first stars in the universe form when chemically pristine gas heats as it falls into dark-matter potential wells, cools radiatively because of the formation of molecular hydrogen, and becomes self-gravitating. Using supercomputer simulations, we demonstrated that the stars' properties depend critically on the currently unknown nature of the dark matter. If the dark-matter particles have intrinsic velocities that wipe out small-scale structure, then the first stars form in filaments with lengths on the order of the free-streaming scale, which can be ~10^{20} meters (~3 kiloparsecs, corresponding to a baryonic mass of ~10^7 solar masses) for realistic "warm dark matter" candidates. Fragmentation of the filaments forms stars with a range of masses, which may explain the observed peculiar element abundance pattern of extremely metal-poor stars, whereas coalescence of fragments and stars during the filament's ultimate collapse may seed the supermassive black holes that lurk in the centers of most massive galaxies.

Most of the matter in the universe does not interact with light except gravitationally. This "dark matter" is usually assumed to be "cold," meaning that its velocity dispersion is sufficiently small for density perturbations imprinted in the early universe to persist up to very small scales. Although this model is able to describe the large-scale distribution of galaxies in impressive detail, it may face problems on the scale of galaxies and below; for example, it may predict too many satellite galaxies (*1*), as well as too-cuspy profiles for the dark-matter halos that surround galaxies (*2*).

Dark matter has yet to be detected in the laboratory, however, and there exist many viable dark-matter candidates from particle physics that are not cold. "Warm" dark matter (WDM) particles have intrinsic thermal velocities, and these motions quench the growth of structure below a "free-streaming" scale (the distance over which a typical WDM particle travels), which depends on the nature of the particle. Because small and dense halos do not form below the free-streaming scale, the dark-matter halos that surround galaxies in a WDM model have far less substructure and are less concentrated as compared with their cold dark matter (CDM) counterparts, which may help alleviate both the satellite and galactic-core problems (*3*). Structures on larger scales are similar in WDM and CDM, and therefore the distribution of galaxies is not affected. The first generation of stars in the universe forms when primordial gas gets compressed by falling into small–dark-matter potential wells (*4*–*7*). Because WDM affects structure formation on such small scales, it may influence how the first stars form; we have performed simulations to analyze this idea in more detail.

Large-scale power in the spectrum of density perturbations causes progenitors of present-day clusters of galaxies to be among the first objects to condense out of the initially almost smooth mass distribution. We studied the early formation stages of such an object by identifying a massive cluster of galaxies in a dark-matter simulation of a large cosmological volume at redshift $z = 0$ and used a multiscale technique (*8*, *9*) to resimulate its formation and evolution with the cosmological hydrodynamics code Gadget-2 (*9*, *10*). Baryons compressed by falling into the developing dark-matter potential wells cool radiatively through molecular hydrogen emission lines (*9*, *11*); we

[1]Institute for Computational Cosmology, Durham University, South Road, Durham DH1 3LE, UK. [2]Department of Physics, University of Antwerp, Groenenborgerlaan 171, B-2020 Antwerpen, Belgium.

*To whom correspondence should be addressed. E-mail: liang.gao@durham.ac.uk